

Wake of color Fields in charged $\mathcal{N} = 4$ SYM plasmas

Yi-hong Gao, Wei-shui Xu, and Ding-fang Zeng *

Institute of Theoretical Physics, Beijing 100080, China

Abstract

The dissipative dynamics of a heavy quark passing through charged thermal plasmas of strongly coupled $\mathcal{N} = 4$ super Yang-Mills theory is studied using AdS/CFT. We compute the linear response of the dilaton field to a test string in the rotating near-extremal D3 brane background, finding the momentum space profile of $\langle \text{tr} F^2 \rangle$ numerically. Our results naively support the wake picture discussed in hep-th/0605292, provided the rotation parameter is not too large.

June 2006

*gaoyh@itp.ac.cn, wsxu@itp.ac.cn, and dfzeng@itp.ac.cn

1 Introduction

According to the AdS/CFT correspondence [1, 2, 3, 4], the physics of a heavy quark passing through finite temperature $\mathcal{N} = 4$ super Yang-Mills plasmas may have the dual description in terms of a fundamental string in the background formed by a stack of near-extremal D3-branes. Such a subject has been studied in a number of recent papers [5, 6, 7, 8, 9, 10, 11, 12, 13, 14, 15, 16], motivated by its possible connection with jet-quenching observed at RHIC [17, 18, 19, 20] in relativistic heavy ion collisions. This remarkable phenomenon can be understood as the strong energy loss of a high energy parton moving through the quark-gluon plasma; for some non-AdS/CFT based theoretical studies, see *e.g.* [21, 22, 23, 25, 24, 26, 27].

In [6][8], the AdS/CFT duality was applied to the computation of the drag force on a moving quark received by a hot $\mathcal{N} = 4$ SYM plasma. The background metric in this dual description comes from near-extremal static D3-branes, which is simply AdS_5 -Schwarzschild $\times S^5$ in the near-horizon limit and corresponds to a neutral quark-gluon plasma. Such a computation was extended to R -charged $\mathcal{N} = 4$ SYM plasmas [9][11], where the background is taken to be the near-horizon geometry of rotating D3 branes, giving rise to the drag force exerted by the thermal plasma with a non-vanishing chemical potential. However, both of these works relied on the test string approximation; back-reaction of such a string on the background was completely neglected. More recently, the authors of [12] have computed linear responses of the dilaton field to a test string in the AdS_5 -Schwarzschild $\times S^5$ background, which takes some back-reaction effects into account. Their result is quite interesting, exhibiting a recoil energy scale in some ranges and a directional peak of gluons radiated from the heavy quark, in consistent with the wake scenarios [25, 27] of jet-quenching. With AdS/CFT, this kind of computations should provide us useful information on the energy loss of heavy quarks passing through the plasma.

In this note we wish to extend the result of [12] to R -charged thermal plasmas, by studying the linear response of the dilaton field to a test string in the rotating near-extremal D3 brane background. We shall treat the neutral plasma as a special case of the charged ones, to see how the profile of $\langle \text{tr } F^2 \rangle$ changes and, in particular, whether a wake form can be found in the presence of charges. For simplicity, we will restrict ourselves to the case where only one angular momentum parameter is non-vanishing [29][30]. The near horizon geometry thus reads

$$\begin{aligned}
 ds^2 = & f^{-\frac{1}{2}}(-hdt^2 + d\vec{x}^2) + f^{\frac{1}{2}}(\tilde{h}^{-1}dr^2 - \frac{2lr_0^2L^2}{r^4\Delta f} \sin^2\theta dt d\phi \\
 & + r^2[\Delta d\theta^2 + \tilde{\Delta} \sin^2\theta d\phi^2 + \cos^2\theta d\Omega_3^2])
 \end{aligned}
 \tag{1}$$

with

$$\begin{aligned}
f &= \frac{L^4}{r^4 \Delta}, \\
\Delta &= 1 + \frac{l^2}{r^2} \cos^2 \theta, \\
\tilde{\Delta} &= 1 + \frac{l^2}{r^2} + \frac{r_0^4 l^2 \sin^2 \theta}{r^6 \Delta f}, \\
h &= \frac{1}{\Delta} \left(1 + \frac{l^2}{r^2} \cos^2 \theta - \frac{r_0^4}{r^4} \right), \\
\tilde{h} &= \frac{1}{\Delta} \left(1 + \frac{l^2}{r^2} - \frac{r_0^4}{r^4} \right)
\end{aligned} \tag{2}$$

and $L^4 = g_{YM}^2 N \alpha'^2$. For later convenience, let us introduce two symbols h_1, h_2

$$h_1 = \left[\frac{1}{2} (\sqrt{l^4 + 4r_0^4} - l^2) \right]^{\frac{1}{2}} \tag{3a}$$

$$h_2 = \left[\frac{1}{2} (\sqrt{l^4 + 4r_0^4} + l^2) \right]^{\frac{1}{2}} \tag{3b}$$

where h_1 is the event horizon. We will consider a classical string placed in the background (1), with one end attached to the boundary of the AdS space moving in a constant velocity v , and the other end attached to the horizon of the black hole at the center of the AdS space. Our purpose here is to compute the linear response of the dilaton in the background metric (1), paying particular attention to the energy scale at which dissipation occurs as well as the existence of directional peaks.

This paper is organized as follows: In section 2 we recall some relevant formulae of [9, 11]. In section 3, we derive a set of differential equations governing linear perturbations of the dilaton field, following [12] closely. Section 4 then applies the relaxation method [28] to the boundary value problem, and presents our numerical results with some discussions. As we will see, in the case of $l = 0$, our results agree with those given in [12], where a different numerical method was used.

2 Test String Solutions

Let us begin with the string configuration

$$X^0 = \tau, \quad X^r = \sigma, \quad X^1 = v\tau + \xi(r), \quad \theta = \theta(r) \tag{4}$$

The function $\xi(r)$ in (4) is determined by

$$\xi' = \frac{vr_0^2}{L^2} \frac{f}{h\tilde{h}} \sqrt{1 + \Delta\tilde{h}r^2\theta'^2} \quad (5)$$

and $\theta(r)$ obeys a complicated equation [9, 11], which in generical (for $l \neq 0$) does not allow constant solutions. However, there are two special cases where $\theta(r)$ can have r -independent solutions, provided $\theta \rightarrow 0$ or $\frac{\pi}{2}$ as $r \rightarrow \infty$. In the first case the string is parallel to the rotation axis, while in the second case the string lies in the plane perpendicular to the rotation axis. In the present paper we will consider the first case only. This string configuration (with $\theta \equiv 0$), though special, is nevertheless non-trivial, since it could be used to study the physical effects of the SYM plasma charge on the test string.

Inserting $\theta \equiv 0$ into (5) gives

$$\xi' = \frac{vr_0^2}{L^2} \frac{f}{h} \Big|_{\theta=0} = \frac{vr_0^2 L^2}{r^4 + r^2 l^2 - r_0^4}. \quad (6)$$

One may write down an explicit expression for $\xi(r)$ by integrating out the above equation. With the definition (3a)-(3b), it is easy to derive:

$$\xi(r) = \frac{vr_0^2 L^2}{\sqrt{l^4 + 4r_0^4}} \left[\frac{\pi}{2h_2} - \frac{1}{h_1} \ln \frac{\sqrt{r+h_1}}{\sqrt{r-h_1}} - \frac{1}{h_2} \arctan \frac{r}{h_2} \right]. \quad (7)$$

Now, to compare this with [8][12], we set

$$z_H = \frac{r_0^2 L^2}{h_1 \sqrt{l^4/4 + r_0^4}} \quad (8)$$

so that

$$\xi(r) = \frac{vz_H}{4} \left[\frac{\pi h_1}{h_2} - \ln \frac{r+h_1}{r-h_1} - \frac{2h_1}{h_2} \arctan \frac{r}{h_2} \right]. \quad (9)$$

Note that Eq.(9) under the limit $l \rightarrow 0$ will become identical to the string configuration

$$\xi(r) = \frac{L^2 v}{2r_0} \left(\frac{\pi}{2} - \arctan \frac{r}{r_0} - \log \sqrt{\frac{r+r_0}{r-r_0}} \right)$$

studied in [8][12]. This could be expected, since in that limiting case the metric (1) reduces exactly to AdS_5 -Schwarzschild. Now for generic $l \neq 0$, the effective 5-dimensional background felt by the string parallel to the rotation axis also gets simplified. Actually, taking $\theta \equiv 0$

and freezing all the angular degrees of freedom in (1) yields:

$$\begin{aligned} ds^2 &= -f^{-1/2}h dt^2 + f^{1/2}h^{-1}dr^2 + f^{-1/2}d\vec{x}^2, \\ f &= \frac{L^4}{r^4 + r^2 l^2}, \quad h = 1 - \frac{r_0^4}{r^4 + r^2 l^2}. \end{aligned} \quad (10)$$

3 Linear Responses of the Dilaton

We turn now to back-reaction of the test string to the background, following the same routine of [12]. Consider the response of the dilaton field ϕ to the test string, where ϕ has non-trivial solutions determined by minimizing the action

$$S = -\frac{1}{4\kappa_5^2} \int dx^5 \sqrt{-G} (\partial\phi)^2 - \frac{1}{2\pi\alpha'} \int_M d^2\sigma e^{\phi/2} \sqrt{-\gamma} \quad (11)$$

with

$$\gamma_{ab} = \partial_a X^\mu \partial_b X^\nu G_{\mu\nu}, \quad \kappa_5^2 = 8\pi G_5 = \frac{4\pi^2 L^3}{N^2}. \quad (12)$$

To establish the equation of motion for ϕ , it is convenient to express the action as a single volume integral [12]

$$S = -\frac{1}{4\kappa_5^2} \int dx^5 \sqrt{-G} \left[(\partial\phi)^2 + \frac{4\kappa_5^2}{2\pi\alpha'} \int_M d^2\sigma e^{\phi/2} \frac{\sqrt{-\gamma}}{\sqrt{-G}} \delta^5(x^\mu - X^\mu(\sigma)) \right]. \quad (13)$$

This gives rise to the linearized equation of motion describing the response of the dilaton to the test string:

$$\square\phi = \frac{1}{\sqrt{-G}} \partial_\mu \sqrt{-G} G^{\mu\nu} \partial_\nu \phi = \frac{\kappa_5^2}{2\pi\alpha'} \int_M d^2\sigma e^{\phi/2} \frac{\sqrt{-\gamma}}{\sqrt{-G}} \delta^5(x^\mu - X^\mu(\sigma)) \equiv J \quad (14)$$

Substituting (4), (6), (7) into the above definition of J and calculating $\sqrt{-\gamma}$ as well as $\sqrt{-G}$ in terms of the metric components, one finds

$$J = \frac{\kappa_5^2}{2\pi\alpha'} \frac{\sqrt{-\gamma}}{\sqrt{-G}} \delta(x^1 - X^1(t, r)) \delta(x^2 - X^2) \delta(x^3 - X^3) \quad (15)$$

$$\sqrt{-G} = \sqrt{-G_{tt} G_{rr} G_{xx}^3} = G_{xx}^{3/2} (\theta \equiv 0)$$

$$\sqrt{-\gamma} = \sqrt{(h - v^2) \tilde{h}^{-1} + h f^{-1} \xi'^2 + \Delta (h - v^2) r^2 \theta'^2} = \sqrt{1 - v^2} \quad (16)$$

Suppose, just as in [12], that ϕ depends on x^1 and t only through the combination $x^1 - vt$. Also, notice that in our string configuration, $\theta \equiv 0$. Hence we can simplify Eq.(14) to

$$\begin{aligned} \partial_r G_{xx}^{3/2} G^{rr} \partial_r \phi + G_{xx}^{3/2} [(G^{xx} + v^2 G^{tt}) \partial_1^2 + G^{xx} (\partial_2^2 + \partial_3^2)] \phi \\ = \frac{\kappa_5^2 \sqrt{1-v^2}}{2\pi\alpha'} \delta(x^1 - vt - \xi(r)) \delta(x^2 - X^2) \delta(x^3 - X^3) \end{aligned} \quad (17)$$

Now, going to the momentum space

$$\phi(t, r, \vec{x}) = \int \frac{d^3 \vec{k}}{(2\pi)^3} e^{i[k_1(x^1 - vt) + ik_2 x^2 + ik_3 x^3]} \phi_k(r), \quad \tilde{\phi}_k(r) \equiv \phi_k(r) \frac{2\pi\alpha'}{\kappa_5^2 \sqrt{1-v^2}} \quad (18)$$

the above equation is transformed into

$$\partial_r [f^{-\frac{5}{4}} h(r) \partial_r \tilde{\phi}_k(r)] - f(r)^{-\frac{1}{4}} \left[\left[1 - \frac{v^2}{h(r)} \right] k_1^2 + k_\perp^2 \right] \tilde{\phi}_k(r) = e^{-ik_1 \xi(r)}, \quad (19)$$

here f and g are given in (10).

It seems not possible to solve Eq.(19) analytically for the full range of r , but nevertheless we can find explicit solutions in two asymptotical regions. The first one is in the near-horizon region, where $r \sim h_1$ and therefore

$$\begin{aligned} f(r) &\rightarrow \frac{L^4}{r_0^4} \\ h(r) &\rightarrow \frac{2h_1(h_1^2 + h_2^2)(r - h_1)}{r_0^4} \equiv h_0(r) \\ \xi(r) &\rightarrow \frac{vz_H}{4} \left[\frac{\pi h_1}{h_2} - \ln \frac{2h_1}{r - h_1} - \frac{2h_1}{h_2} \arctan \frac{h_1}{h_2} \right] \end{aligned} \quad (20)$$

In this limit (19) reduces to

$$\begin{aligned} \frac{r_0^5 h_0}{L^5} \partial_r (r - h_1) \partial_r \tilde{\phi}_k(r) + \frac{v^2 r_0}{L h_0 (r - h_1)} k_1^2 \tilde{\phi}_k(r) \\ = \exp \left[\frac{-ivk_1 z_H}{4} \left(\frac{\pi h_1}{h_2} - \ln \frac{2h_1}{r - h_1} - \frac{2h_1}{h_2} \arctan \frac{h_1}{h_2} \right) \right]. \end{aligned} \quad (21)$$

Now let

$$Y = \ln \frac{r - h_1}{h_1}, \quad P = \frac{\pi h_1}{h_2} - \ln 2 - \frac{2h_1}{h_2} \arctan \frac{h_1}{h_2}, \quad (22)$$

we can rewrite the above differential equation as

$$\partial_Y^2 \tilde{\phi}_k(Y) + \left[\frac{vk_1 z_H}{4} \right]^2 \tilde{\phi}_k = \frac{z_H h_1 L^3}{4r_0^3} e^Y e^{-ivk_1 z_H(Y+P)/4} \quad (23)$$

The general solution of Eq.(23) thus takes the form

$$\tilde{\phi}_{k,NH}(r) = \frac{z_H h_1 L^3}{4r_0^3} \frac{e^Y e^{-ivk_1 z_H(Y+P)/4}}{1 - ivk_1 z_H/2} + C_k^+ e^{ivk_1 z_H Y/4} + C_k^- e^{-ivk_1 z_H Y/4} \quad (24)$$

where C_k^\pm are arbitrary constants. In this near horizon region, we require ϕ depend on t and Y through the combination $t + vk_1 z_H Y/4$ only, so we can set $C_k^+ = 0$. Physically this means that we accept the infalling solution while reject the outgoing one.

Next we consider asymptotical solutions in region near the (AdS) boundary, where

$$r \rightarrow \infty, \quad f^{-\frac{1}{4}} \rightarrow \frac{r}{L}, \quad h \rightarrow 1 \quad (25)$$

In that region, Eq.(19) becomes

$$\frac{1}{r} \partial_r r^5 \partial_r \tilde{\phi}_k(r) = \frac{L^5}{r} \quad (26)$$

whose general solution has the form:

$$\tilde{\phi}_{k,NB}(r) = -\frac{1}{3} L^5 r^{-3} + A_k + B_k r^{-4} \quad (27)$$

The constant A_k should be set to zero, as there are no deformations in the dilaton Lagrangian. Physically we will be interested in B_k , since according to AdS/CFT, this quantity is directly related to the vacuum expectation value of the operator $\mathcal{O}_{F^2} \sim \text{tr} F^2$ coupled to the dilaton. Actually, using the AdS/CFT dictionary we can write the VEV as

$$\langle \mathcal{O}_{F^2}(t, \vec{x}) \rangle = \frac{1}{2\kappa_5^2} \lim_{r \rightarrow \infty} \sqrt{-g} g^{rr} \partial_r \phi = -\frac{1}{2\kappa_5^2} \lim_{r \rightarrow \infty} \frac{r^5}{L^5} \partial_r \phi(t, \vec{x}, r) \quad (28)$$

where the metric (10) has been applied. Note that the above limit does not exist due to the first term in Eq.(27). Since such a term does not depend on \vec{k} , transforming it into real space will lead to a delta function supported at the quark location, which should be subtracted [12]. The correspondence between $\langle \mathcal{O}_{F^2} \rangle$ and $\phi(t, \vec{x}, r)$ in (28) should now be understood as

a relation after the delta-function subtraction. We thus find:

$$\langle \mathcal{O}_{F^2}(t, \vec{x}) \rangle = -\frac{\sqrt{1-v^2}}{4\pi\alpha' L^5} \int \frac{d^3\vec{k}}{(2\pi)^3} e^{ik_1(x^1-vt)+ik_2x^2+ik_3x^3} B_k. \quad (29)$$

Now, as in the neutral plasma case [12], further subtraction is needed in order to separate the dissipative dynamics from the near field contributions of the quark. One expects that these near field contributions correspond to the string hanging straight down in AdS_5 . Thus, when $v = 0$, we can apply the method of [31] directly to derive

$$\langle \mathcal{O}_{F^2}(t, x) \rangle^{\text{near field}} = \frac{1}{16\pi^2} \frac{\sqrt{Ng_{YM}^2}}{|\vec{x}|^4}. \quad (30)$$

Comparing this with (29) for $v = 0$, one gets

$$B_k^{\text{near field}} = \frac{\pi\alpha' L^5 \sqrt{Ng_{YM}^2}}{16} \sqrt{k_1^2 + k_\perp^2}. \quad (31)$$

In the case of $v \neq 0$, the near field contributions are obtainable through a Lorentz boost to the string configuration. The result reads

$$B_k^{\text{near field}} = \frac{\pi L^7}{16} \sqrt{(1-v^2)k_1^2 + k_\perp^2}, \quad (32)$$

which will be subtracted from the numerical values of B_k computed in the next section.

4 Numerical Results and Discussions

We are now in a position to solve the following boundary value problem numerically:

$$\partial_r [f^{-\frac{5}{4}} h(r) \partial_r \tilde{\phi}_k(r)] - f(r)^{-\frac{1}{4}} \left[1 - \frac{v^2}{h(r)} \right] k_1^2 + k_\perp^2 \tilde{\phi}_k(r) = e^{-ik_1 \xi(r)} \quad (33a)$$

$$\tilde{\phi}_k(r) \xrightarrow{r \sim h_1} \frac{z_H h_1 L^3 e^Y e^{-ivk_1 z_H (Y+P)/4}}{4r_0^3} + C_k^- e^{-ivk_1 z_H Y/4} \equiv \tilde{\phi}_{k,NH1} + \tilde{\phi}_{k,NH2} \quad (33b)$$

$$\tilde{\phi}_k(r) \xrightarrow{r \sim \infty} -\frac{1}{3} L^5 r^{-3} + B_k r^{-4} \equiv \tilde{\phi}_{k,NB1} + \tilde{\phi}_{k,NB2} \quad (33c)$$

To this end, we need to implement the boundary conditions at $r \sim h_1$ and $r \sim \infty$, and this can be done by introducing two Wronskians, $W_{NH}(r)$ and $W_{NB}(r)$, to measure the differences between our numerically evaluated $\tilde{\phi}_k(r)$ and the asymptotical solutions (24), (27) found in

the last section. One thus defines, following [12],

$$\begin{aligned} W_{NH}(r) &= (\tilde{\phi}_k - \tilde{\phi}_{k,NH1})\tilde{\phi}'_{k,NH2} - (\tilde{\phi}'_k - \tilde{\phi}'_{k,NH1})\tilde{\phi}_{k,NH2} \\ W_{NB}(r) &= (\tilde{\phi}_k - \tilde{\phi}_{k,NB1})\tilde{\phi}'_{k,NB2} - (\tilde{\phi}'_k - \tilde{\phi}'_{k,NB1})\tilde{\phi}_{k,NB2} \end{aligned} \quad (34)$$

The boundary conditions can then be imposed properly by the requirements $W_{NH}(r) = 0$ at $r \sim h_1$ and $W_{NB}(r) = 0$ at $r \sim \infty$.

The numerical recipes we used in solving the boundary value problem (33) is the standard relaxation method [28]. In programming, we changed the variable $r \rightarrow y \equiv h_1/r$, so that the integration range becomes $y \in (0, 1)$, where $y \sim 1$ corresponds to the horizon and $y \sim 0$ to the AdS_5 boundary. Since the solution has oscillating behavior at $y \approx 1$, we divided the the integration region into four intervals, $(1, 0.9]$, $(0.9, 0.7]$, $(0.7, 0.4]$ and $(0.4, 0)$, and then divided the first, second, third, and fourth intervals into 4096, 1024, 256, and 64 integration steps, respectively, in order to reach as high precision as possible while keeping CPU time in an acceptable range. We also checked that if the whole integration region is divided into 50000 steps uniformly, one can get almost the same results and, of course, this costs more CPU time.

Since Eq.(33a) becomes singular as $r \rightarrow h_1$ or $r \rightarrow \infty$, we have to set $W_{NH} = 0$ at a point very close to the horizon, and set $W_{NB} = 0$ at a large but finite value of r . The conditions imposed in our computations are

$$W_{NH}|_{r=1.001h_1} = 0, \quad W_{NB}|_{r=700h_1} = 0. \quad (35)$$

We depict our numerical results in Fig.1–2, where equi-value lines of $\text{Re}B_k$, $-\text{Im}B_k$, $|B_k|$ etc., for some different values of v and l , are plotted in the momentum plane $k = (K_1, K_\perp)$. In all the plots the near field contributions (32) have been subtracted. We adopt the convention of [12], representing values closest to zero by white regions, and representing the most positive values by black regions. To compare our results with those of [12], we fixed the energy scale explicitly, by setting the temperature of the plasma

$$T = \frac{h_1}{2\pi L^2 r_0^2} \sqrt{l^4 + 4r_0^2} \quad (36)$$

to be $T = 1/\pi \text{ GeV} = 318 \text{ MeV}$, in accordance with the choice made in [12]. Thus, the wave numbers k displayed here are measured by GeV/c . Apart from this, the rotation parameter l is shown in units of h_1 , namely, when we say $l = 0.5$, we actually mean $l = 0.5h_1$.

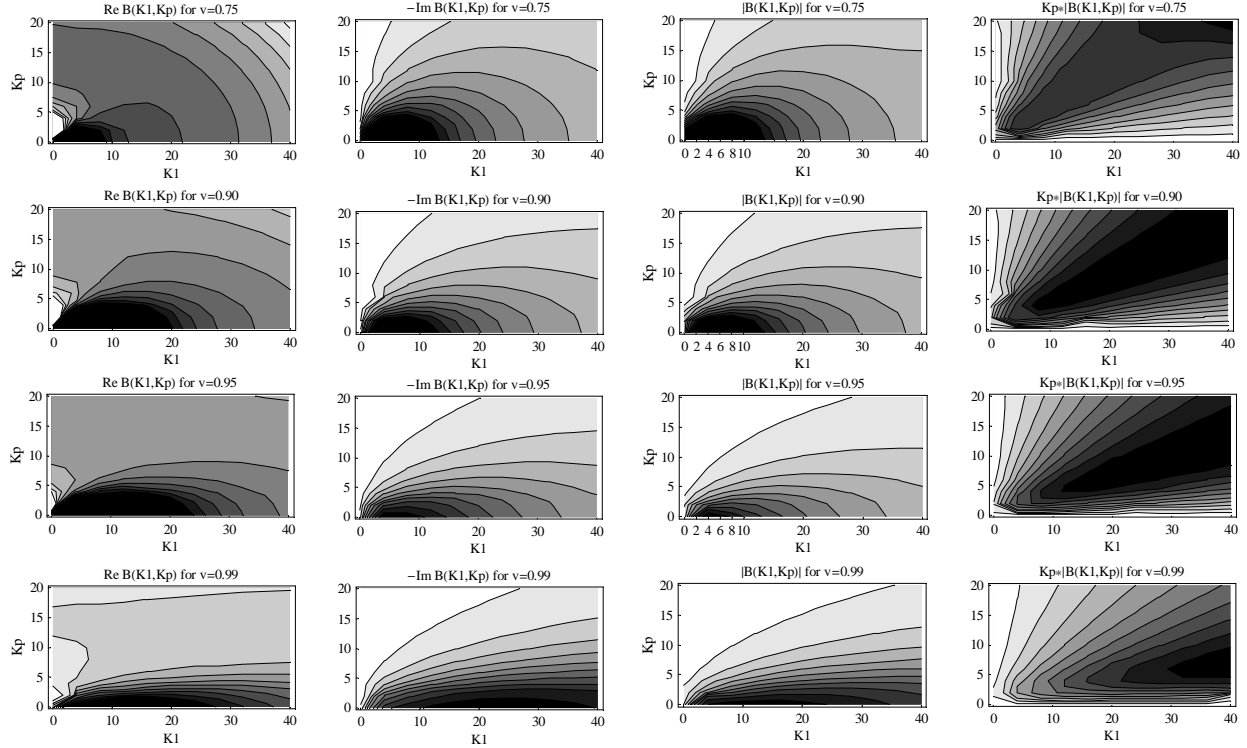


Figure 1: Distributions of equi-value lines of $\text{Re}B(K_1, K_\perp)$, $-\text{Im}B(K_1, K_\perp)$, $|B(K_1, K_\perp)|$, and $K_\perp|B(K_1, K_\perp)|$ in the momentum plane (K_1, K_\perp) , for angular momentum $l = 0$, at speeds $v = 0.75, 0.90, 0.95, 0.99$. We have subtracted the near field contribution (32) from $B(K_1, K_\perp)$.

Fig.1 shows our results of $B_k = B(K_1, K_\perp)$ in the special case $l = 0$. This corresponds to the neutral plasma studied in [12]. The first two columns contain plots of $\text{Re}B(K_1, K_\perp)$ and $-\text{Im}B(K_1, K_\perp)$ at $v = 0.75, 0.90, 0.95, 0.99$, while the third and fourth show the corresponding plots of $|B(K_1, K_\perp)|$ and $K_\perp|B(K_1, K_\perp)|$, respectively. Comparing these with the plots given in [12], one sees that the basic features are the same, both exhibiting a directionally peaked structure in $K_\perp|B(K_1, K_\perp)|$ and a possible range of the recoil energy. For example, focusing on the third line, third column of Fig.1, we find that $|B(K_1, K_\perp)|$ (for $v = 0.95$) is peaked at

$$K_\perp \approx 0, \quad 3 \leq K_1 \leq 7.2 \text{ GeV}/c,$$

which indicates that the recoil energy E_r is in the range $1.5 \leq E_r \leq 3.6 \text{ GeV}$, less than the value

$$E_f = \frac{1 + v^2}{1 - v^2} T = 6.2 \text{ GeV} \quad (\text{for } v = 0.95)$$

predicted in the corresponding free field theory by a factor of a few. This agrees perfectly

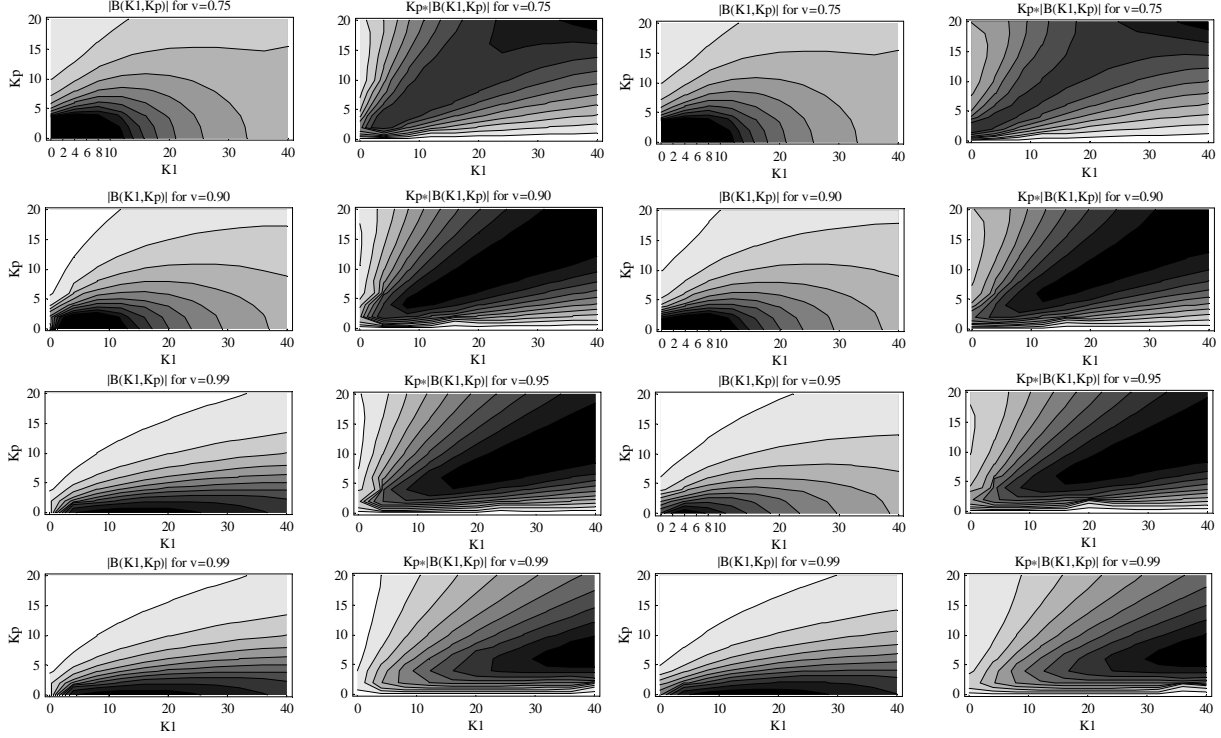


Figure 2: Distributions of equi-value lines of $|B(K_1, K_\perp)|$ and $K_\perp|B(K_1, K_\perp)|$ in the plane (K_1, K_\perp) , for angular momentum $l = 0.5$ and 1 , at speeds $v = 0.75, 0.90, 0.95, 0.99$. We have subtracted the near field contribution (32) from $B(K_1, K_\perp)$. The left eight ones are plots of $|B(K_1, K_\perp)|$ and $K_\perp|B(K_1, K_\perp)|$ for $l = 0.5h_1$, and the right eight ones are the corresponding plots for $l = 1.0h_1$.

with the numerical result of [12].

Now we turn to the case $l \neq 0$. When $l = 0.5$ and 1 , our results for $B(K_1, K_\perp)$ (at speeds $v = 0.75, 0.90, 0.95, 0.99$) are displayed in Fig.2. The first and third columns give the plots of $|B(K_1, K_\perp)|$ for $l = 0.5$ and $l = 1$, respectively. From these plots, one sees that there may exist a finite range of K_\perp in which $|B(K_1, K_\perp)|$ is peaked, just as in the $l = 0$ case. Taking the plot for $l = 1$ at $v = 0.95$ as an example (the one placed at the third line, third column of Fig.2), we find that $|B(K_1, K_\perp)|$ has a peak within

$$K_\perp \approx 0, \quad 2 \leq K_1 \leq 7.6 \text{ GeV}/c,$$

so that the recoil energy E_r is roughly in the range $1 \leq E_r \leq 3.8$ GeV, which is slightly larger than the result found in the $l = 0$ case. That the range of E_r (in particular its upper bound value) becomes larger when l increases seems to be a generic phenomenon in our numerical computations. A possible implication is that the more is the charge carried by the plasma,

the more energy of the quark would be dissipated away by radiation of gluons. This should not be taken too seriously, however, since our numerical results may contain more errors as l becomes larger; see the discussion for $l = 2$ below.

The fourth column of Fig.2 shows plots of $K_{\perp}|B(K_1, K_{\perp})|$ for $l = 1$, at speeds $v = 0.75, 0.90, 0.95,$ and 0.99 . Again, we can clearly see a directionally peaked structure in these plots, much resembling the $l = 0$ case. We have also displayed plots of $K_{\perp}|B(K_1, K_{\perp})|$ for $l = 0.5$ in the second column of Fig.2, finding that they look quite similar to (and in fact, they are intermediate between) those in the $l = 0, 1$ cases. Thus, at least for $l \leq 1$, our results suggest that the wake picture described in [12] may also apply to R -charged plasmas.

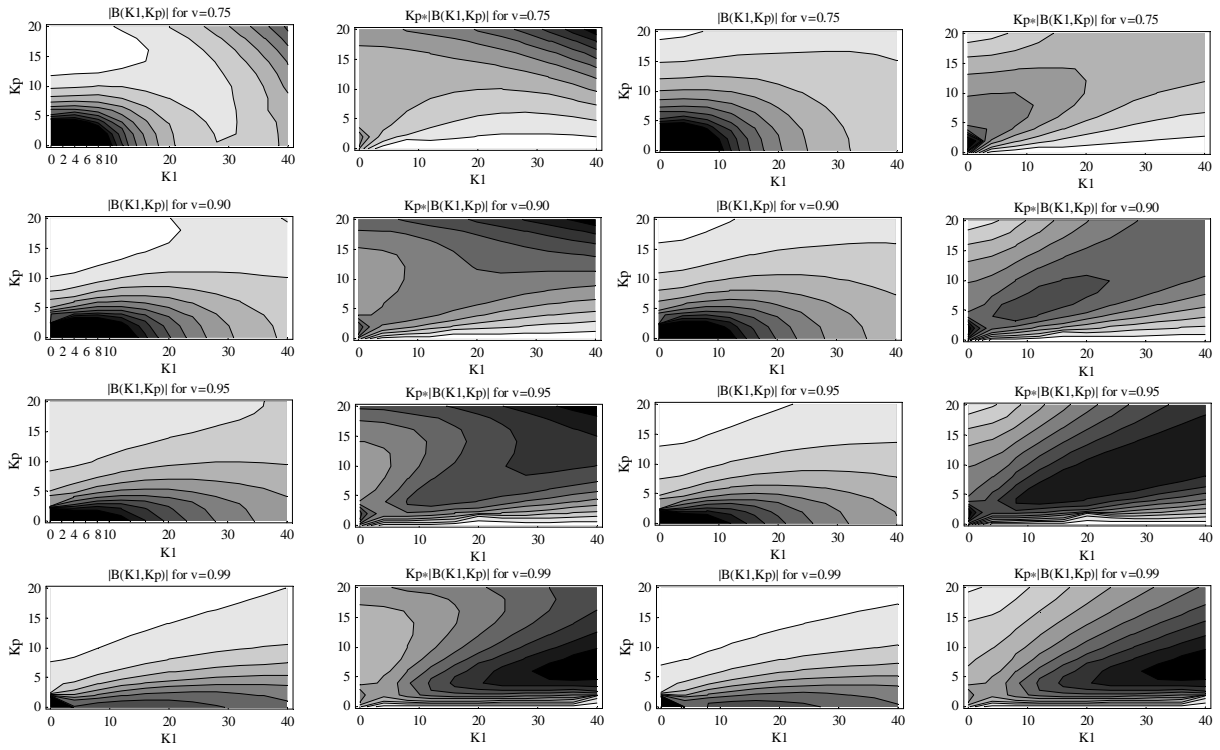


Figure 3: Distributions of equi-value lines of $|B(K_1, K_{\perp})|$ and $K_{\perp}|B(K_1, K_{\perp})|$ in the plane (K_1, K_{\perp}) , for $l = 2$, at speeds $v = 0.75, 0.90, 0.95, 0.99$. The near field contribution (32) has been subtracted from $B(K_1, K_{\perp})$. The left eight plots are computed using the boundary conditions (35), while the right eight ones are the corresponding plots with the new boundary conditions $W_{NH}|_{r=1.001h_1} = 0, W_{NB}|_{r=800h_1} = 0$ imposed.

What would happen if l becomes larger? For a comparison, the plots of $|B(K_1, K_{\perp})|$ and $K_{\perp}|B(K_1, K_{\perp})|$ for $l = 2$ are displayed in the first and second columns of Fig.3. The pattern of such plots appears now to be somehow different from what we have seen in the case of $l \leq 1$. In particular, at relatively low speeds, the directionally peaked structure in $K_{\perp}|B(K_1, K_{\perp})|$ seems no longer obvious. We should mention that in our numerical calculations, plot patterns

for l being larger will depend more sensitively on how we impose the boundary conditions. For instance, if we modify the second condition in (35) by setting $W_{NB} = 0$ at $r = 800h_1$ instead of $700h_1$, then the plots for $l = 2$ will have a new pattern, as shown in the third and fourth columns of Fig.3, which is different from the previous one. Similar changes in plots are also observed at $l = 0, 0.5$ and 1 , but they are far less remarkable, leaving the pattern qualitatively the same. Hence, our numerical results for $l = 2$ are not quite reliable, which may contain more errors than those in the $l \leq 1$ case.

Following [12], we can determine the opening angle θ between the velocity of the heavy quark and the directional peak found in $K_{\perp}B(K_{\perp}, K_{\perp})$. The results are summarized in the following table:

θ	$v = 0.75$	$v = 0.90$	$v = 0.95$	$v = 0.99$
$l = 0$	0.59	0.42	0.28	0.17
$l = 0.5$	0.57	0.39	0.27	0.16
$l = 1$	0.55	0.37	0.26	0.15

(37)

We thus find a strong dependence of θ on v in both the neutral and charged cases. For fixed v , however, the opening angle depends rather weakly on l (at least in the region $l \leq 1$; as we mentioned, our numerical results for $l = 2$ are not quite trustable), in a monotonically decreasing way.

In conclusions, we have studied the dissipative dynamics of a heavy quark passing through charged $\mathcal{N} = 4$ SYM plasmas. Neutral plasmas were treated as a special case of the charged ones, where we reproduced the main results of [12] using a different numerical method. Our results for $l \leq h_1$ naively support the wake picture, but they are inconclusive for $l \sim 2h_1$ due to numerical errors.

References

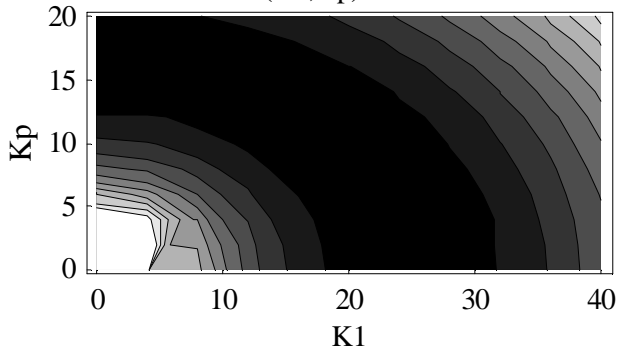
- [1] J. M. Maldacena, “The large N limit of superconformal field theories and supergravity,” *Adv. Theor. Math. Phys.* **2** (1998) 231–252, [hep-th/9711200](#).
- [2] S. S. Gubser, I. R. Klebanov, and A. M. Polyakov, “Gauge theory correlators from non-critical string theory,” *Phys. Lett.* **B428** (1998) 105–114, [hep-th/9802109](#).
- [3] E. Witten, “Anti-de Sitter space and holography,” *Adv. Theor. Math. Phys.* **2** (1998) 253–291, [hep-th/9802150](#).

- [4] E. Witten, “Anti-de Sitter space, thermal phase transition, and confinement in gauge theories,” *Adv. Theor. Math. Phys.* **2** (1998) 505–532, [hep-th/9803131](#).
- [5] H. Liu, K. Rajagopal, and U. A. Wiedemann, “Calculating the jet quenching parameter from AdS/CFT,” [hep-ph/0605178](#).
- [6] C. P. Herzog, A. Karch, P. Kovtun, C. Kozcaz, and L. G. Yaffe, “Energy loss of a heavy quark moving through $N = 4$ supersymmetric Yang-Mills plasma,” [hep-th/0605158](#).
- [7] A. Buchel, “On jet quenching parameters in strongly coupled non-conformal gauge theories,” [hep-th/0605178](#).
- [8] S. S. Gubser, “Drag force in AdS/CFT,” [hep-th/0605182](#).
- [9] C. P. Herzog, “Energy Loss of Heavy Quarks from Asymptotically AdS Geometries,” [hep-th/0605191](#).
- [10] J. Casalderrey-Solana and D. Teaney, “Heavy quark diffusion in strongly coupled $N = 4$ Yang Mills,” [hep-ph/0605199](#).
- [11] E. Caceres and A. Guijosa, “Drag Force in Charged $N=4$ SYM Plasma,” [hep-th/0605235](#).
- [12] J. J. Friess, S. S. Gubser, G. Michalogiorgakis, “Dissipation from a heavy quark moving through $\mathcal{N} = 4$ super-Yang-mills plasma”, [hep-th/0605292](#).
- [13] E. Cáceres and A. Güijosa, “On Drag Forces and Jet Quenching in Strong-Coupled Plasmas” [hep-th/0606134](#).
- [14] Feng-Li Lin and T. Matsuo, “Jet Quenching Parameter in Medium with Chemical Potential from AdS/CFT”, [hep-th/0606136](#).
- [15] S. D. Avramis and K. Sfetsos, “Supergravity and the jet quenching parameter in the presence of R-charge densities”, [hep-th/0606190](#).
- [16] N. Armesto, J. D. Edelstein, and J. Mas, “Jet quenching at finite ‘t Hooft coupling and chemical potential from AdS/CFT”, [hep-ph/0606245](#).
- [17] **BRAHMS** Collaboration, I. Arsene *et. al.*, “Quark gluon plasma and color glass condensate at RHIC? The perspective from the BRAHMS experiment,” *Nucl. Phys.* **A757** (2005) 1–27, [nucl-ex/0410020](#).

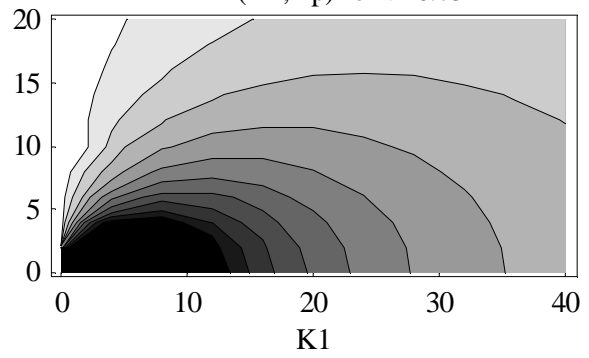
- [18] **PHENIX** Collaboration, K. Adcox *et. al.*, “Formation of dense partonic matter in relativistic nucleus nucleus collisions at RHIC: Experimental evaluation by the PHENIX collaboration,” *Nucl. Phys.* **A757** (2005) 184–283, [nucl-ex/0410003](#).
- [19] B. B. Back *et. al.*, “The PHOBOS perspective on discoveries at RHIC,” *Nucl. Phys.* **A757** (2005) 28–101, [nucl-ex/0410022](#).
- [20] **STAR** Collaboration, J. Adams *et. al.*, “Experimental and theoretical challenges in the search for the quark gluon plasma: The STAR collaboration’s critical assessment of the evidence from RHIC collisions,” *Nucl. Phys.* **A757** (2005) 102–183, [nucl-ex/0501009](#).
- [21] V. Greco, C. M. Ko, and P. Levai, “Parton coalescence and antiproton/pion anomaly at RHIC,” *Phys. Rev. Lett.* **90** (2003) 202302, [nucl-th/0301093](#).
- [22] R. C. Hwa and C. B. Yang, “Recombination of shower partons at high p(T) in heavy-ion collisions,” *Phys. Rev.* **C70** (2004) 024905, [nucl-th/0401001](#).
- [23] A. Majumder, E. Wang, and X.-N. Wang, “Modified dihadron fragmentation functions in hot and nuclear matter,” [nucl-th/0412061](#).
- [24] N. Armesto, C. A. Salgado, and U. A. Wiedemann, “Measuring the collective flow with jets,” *Phys. Rev. Lett.* **93** (2004) 242301, [hep-ph/0405301](#).
- [25] R. J. Fries, S. A. Bass, and B. Muller, “Correlated emission of hadrons from recombination of correlated partons,” *Phys. Rev. Lett.* **94** (2005) 122301, [nucl-th/0407102](#).
- [26] J. Casalderrey-Solana, E. V. Shuryak, and D. Teaney, “Conical flow induced by quenched QCD jets,” *J. Phys. Conf. Ser.* **27** (2005) 22–31, [hep-ph/0411315](#).
- [27] J. Ruppert and B. Muller, “Waking the colored plasma,” *Phys. Lett.* **B618** (2005) 123–130, [hep-ph/0503158](#).
- [28] W. H Press et al, “Numerical Recipes in C”, second edition, Cambridge University Press 1993.
- [29] J. G. Russo, “New compactifications of supergravities and large N QCD”, *Nucl. Phys.* **B543** (1999) 183, [hep-th/9808117](#).
- [30] M. Cvetič and S. S. Gubser, “Phases of R-charged black holes, spinning branes and strongly coupled gauge theories”, *JHEP* **9903**, 003 (1999), [hep-th/9902195](#).

- [31] U. H. Danielsson, E. Keski-Vakkuri, and M. Kruczenski, “Vacua, propagators, and holographic probes in AdS/CFT,” *JHEP* **01** (1999) 002, [hep-th/9812007](#).

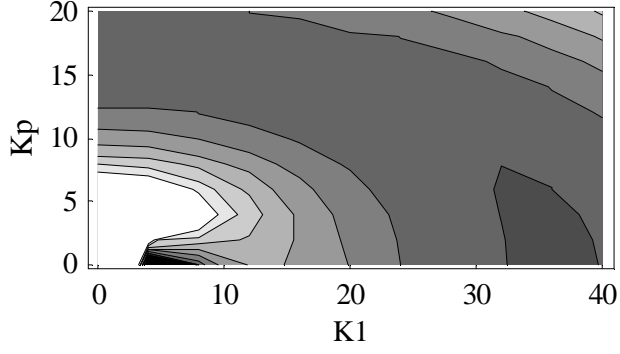
Re B(K1,Kp) for $\nu=0.75$



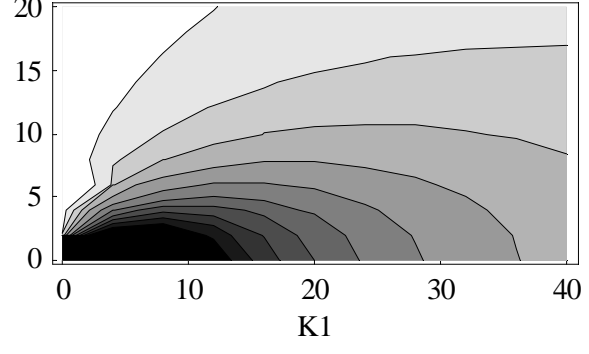
$-\text{Im} B(K_1, K_p)$ for $\nu=0.75$



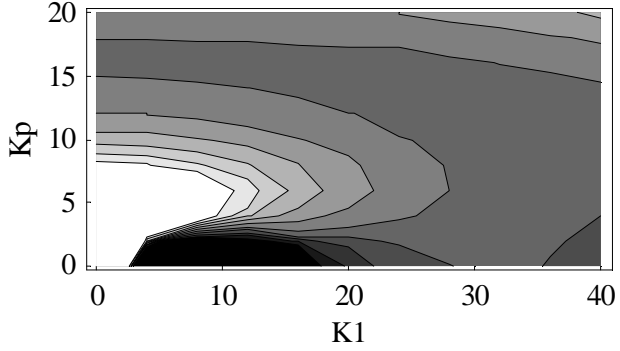
Re B(K1,Kp) for $\nu=0.90$



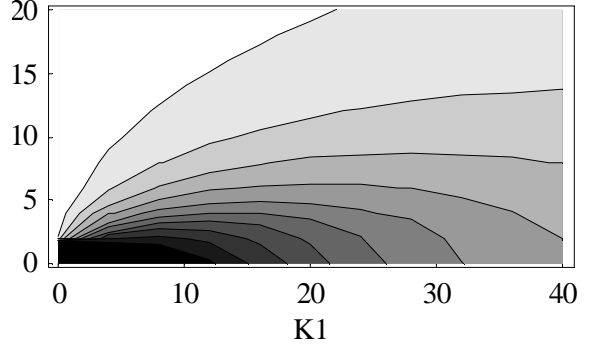
$-\text{Im} B(K_1, K_p)$ for $\nu=0.90$



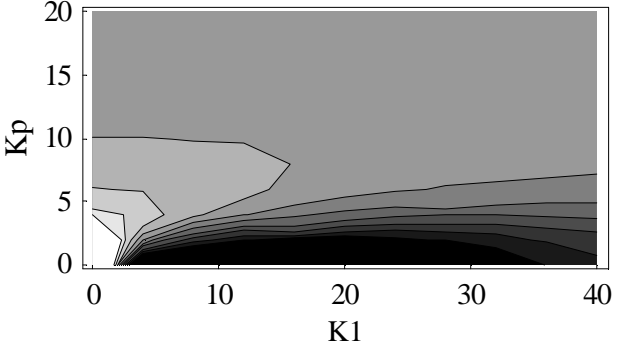
Re B(K1,Kp) for $\nu=0.95$



$-\text{Im} B(K_1, K_p)$ for $\nu=0.95$



Re B(K1,Kp) for $\nu=0.99$



$-\text{Im} B(K_1, K_p)$ for $\nu=0.99$

